Spectrochimica Acta Part A: Molecular and Biomolecular Spectroscopy 116 (2013) 451–459

Contents lists available at ScienceDirect

Spectrochimica Acta Part A: Molecular and Biomolecular Spectroscopy

journal homepage: www.elsevier.com/locate/saa

The infrared, Raman, NMR and UV spectra, ab initio calculations and spectral assignments of 2-amino-4-chloro-6-methoxypyrimidine

Z. Cinar [a], M. Karabacak [b], M. Cinar [c], M. Kurt [d], P. Chinna babu [e], N. Sundaraganesan [e,*]

[a] Department of Physics, Afyon Kocatepe University, 03040 Afyonkarahisar, Turkey
[b] Department of Mechatronics Engineering, H.F.T. Technology Faculty, Celal Bayar University, 45400 Turgutlu, Manisa, Turkey
[c] Department of Science Education, Bayburt University, 69000 Bayburt, Turkey
[d] Department of Physics, Ahi Evran University, 40100 Kırsehir, Turkey
[e] Department of Physics (Engg.), Annamalai University, Annamalai Nagar, 608 002 Chidambaram, Tamil Nadu, India

HIGHLIGHTS

- The FT-IR and FT-Raman spectra of ACMP were recorded.
- The vibrational frequencies were calculated by DFT method and compared with experimental values.
- ^{13}C, ^{1}H and DEPT 135 NMR analysis were also carried out.
- UV spectrum were recorded and compared with calculated ones.

GRAPHICAL ABSTRACT

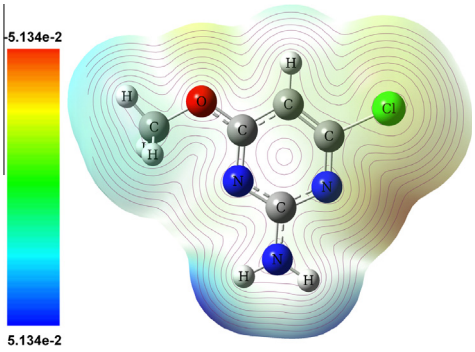

ARTICLE INFO

Article history:
Received 28 April 2013
Received in revised form 4 July 2013
Accepted 21 July 2013
Available online 30 July 2013

Keywords:
DFT
Vibrational spectra
NMR
Electronic properties
2-Amino-4-chloro-6-methoxypyrimidine

ABSTRACT

The 2-amino-4-chloro-6-methoxypyrimidine abbreviated as ACMP have been investigated by both the experimental and theoretical methods; through this work we provide the essential fact about the structural and vibrational insights. The optimized molecular structure, atomic charges, vibrational frequencies and ultraviolet spectral interpretation of ACMP have been studied by performing DFT/B3LYP/6-311++G(df,pd) level of theory. The FT-IR, FT-Raman spectra were recorded in the region 4000–400 cm^{-1} and 4000–50 cm^{-1} respectively. The UV absorption spectrum of the compound that dissolved in ethanol and water solution were recorded in the range of 200–400 nm. The scaled wavenumbers are compared with the experimental values. The difference between the observed and scaled wavenumber values of most of the fundamentals is very small. Based on the UV spectrum and TD-DFT calculations, the electronic structure and the assignments of the absorption bands were carried out. The ^{1}H, ^{13}C and DEPT 135 nuclear magnetic resonance (NMR) chemical shifts of the molecule were calculated using with the Gauge Including Atomic Orbital (GIAO) method and compared with experimental results. Besides, molecular electrostatic potential (MEP), frontier molecular orbitals (FMO) analysis were investigated using theoretical calculations.

Introduction

Pyrimidine metabolism was investigated at various stages of somatic embryo development of white spruce (Picea glauca). The pyrimidine ring system has wide occurrence in nature as substituted and ring fused compounds and derivatives, including the nucleotides, thiamine (vitaminB1) and alloxan [1]. It is also found in many synthetic compounds such as barbiturates and the HIV drug, zidovudine. Pyrimidine and purine containing compounds play a significant role in many biological systems [2–4], where both exist in nucleic acids, several vitamins, coenzymes and antibiotics. Heterocycles are ubiquitous to among pharmaceutical

* Corresponding author. Tel.: +91 9442068405.
E-mail address: sundaraganesan_n@yahoo.com (N. Sundaraganesan).

1386-1425/$ - see front matter © 2013 Elsevier B.V. All rights reserved.
http://dx.doi.org/10.1016/j.saa.2013.07.044

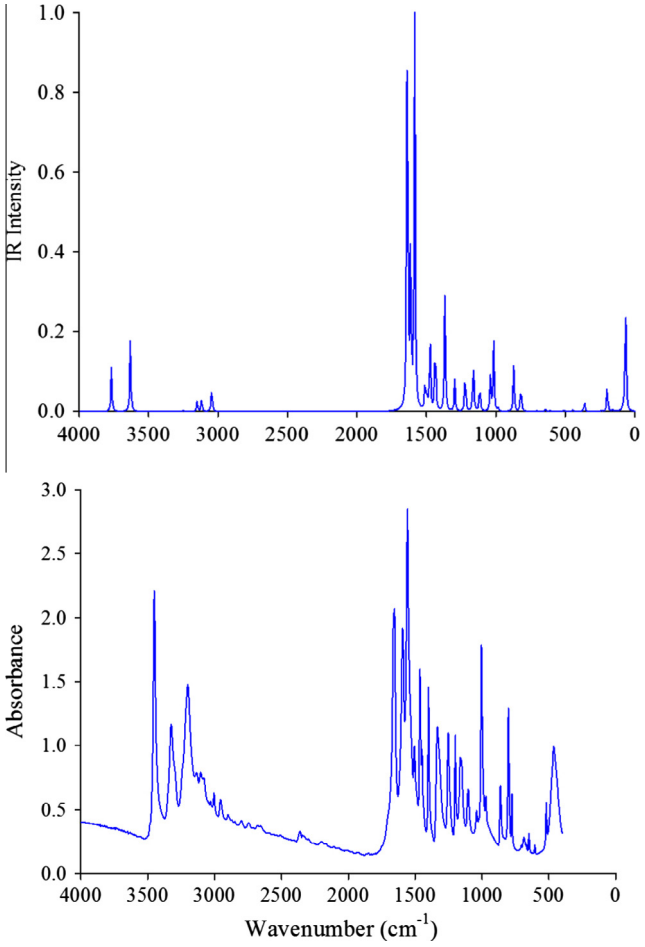

Fig. 1. Comparison of experimental and theoretical (6-311++G(df,pd)) FT-IR spectra for ACMP.

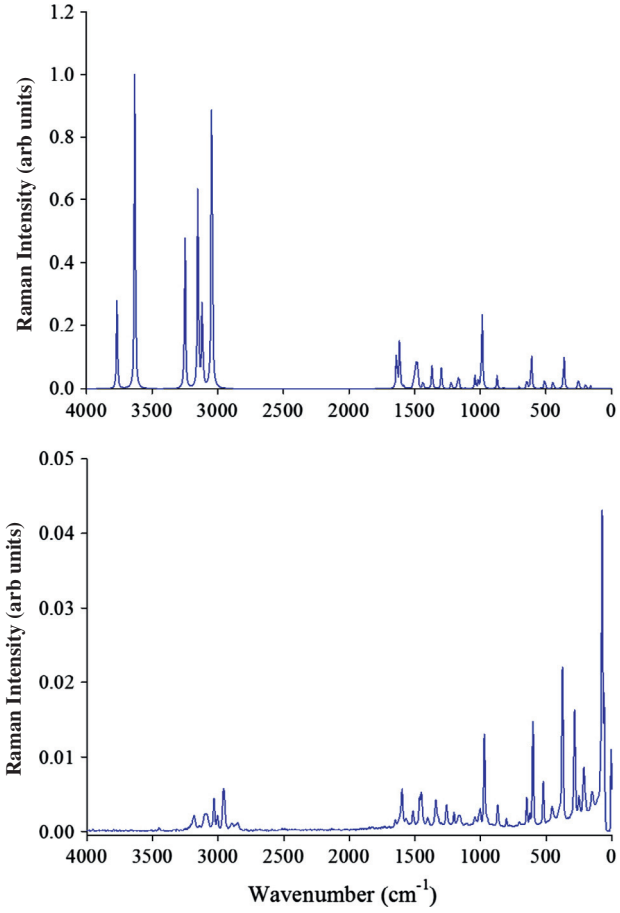

Fig. 2. Comparison of experimental and theoretical (6-311++G(df,pd)) FT-Raman spectra for ACMP.

compounds [5]. Pyrimidine moiety is an important class of N-containing heterocycles widely used as key building blocks for pharmaceutical agents.

The electronic absorption spectra of different pyrimidine derivatives such as 4,6-dichloro-pyrimidine, 4,6-dichloro, 5-amino-pyrimidine, 2,4,6-trichloro-pyrimidine, 4,6-dihydroxy-pyrimidine, 4,6-dihydroxy-5-nitro-pyrimidine, 2,4-diamino-pyrimidine, 2,4-diamino-6-hydroxy-pyrimidine, 2,4-dihydroxy-5-carboxy-pyrimidine, 2,4-dimethyl-6-hydroxy-pyrimidine, 5-nitro-uracil, and orotic acid have been measured experimentally and calculated theoretically by Mogren et al. [6]. Recently, our group reported vibrational spectra, UV and NMR, first order hyperpolarizability and HOMO–LUMO analysis of a similar molecule 2-amino-4-chloro-6-methylpyrimidine [7]. However, to the best of our knowledge the quantum chemical calculations and the vibrational spectra of the title compound have not been reported up to now.

This inadequacy which observed in the literature encouraged us to do this theoretical and experimental vibrational spectroscopic research to give a correct assignment of the fundamental bands in the experimental FT-IR and FT-Raman spectra on the basis of the calculated total energy distribution (TED). In this paper we carried out a more complete and reliable assignment of the vibrational spectra of 2-amino-4-chloro-6-methoxypyrimidine. Thus we first performed geometry optimization calculations for the title molecule using DFT/B3LYP method with 6-311++G(df,pd) as basis set. These calculations are valuable for providing insight into molecular parameters and the vibrational spectra. The aim of this work is to explore the molecular dynamics and the structural parameters that govern the chemical behavior, and to compare predictions made from theory with experimental observations.

Experimental details

The sample was purchased from Sigma–Aldrich Company with a stated purity 98% and it was used as such without further purification. The FT-IR spectrum of compound was recorded in the region 400–4000 cm^{-1} on a Perkin Elmer FT-IR System Spectrum BX spectrometer calibrated using polystyrene bands. The sample was prepared using a KBr disc technique because of solid state. FT-Raman spectrum was recorded using 1064 nm line of Nd:YAG laser as excitation wave length in the region 50–4000 cm^{-1} on a Bruker RFS 100/S FT-Raman. The detector is a liquid nitrogen cooled Ge detector. Five hundred scans were accumulated at 4 cm^{-1} resolution using a laser power of 100 mW. The ^{1}H, ^{13}C and DEPT NMR spectra were recorded in DMSO solution on a Brucker DPX 400 MHz spectrometer using tetramethylsilane (TMS) as an internal reference at 25 °C. The UV absorption spectrum were recorded in ethanol and water solution on Shimadzu UV-1800 PC spectrophotometer in the spectral region of 200–400 nm. The measured FT-IR, FT-Raman, theoretically constructed FT-IR and FT-Raman spectra are shown in Figs. 1 and 2.

Computational details

In the present work, the density functional theory (DFT/B3LYP) at the 6-311++G(df,pd) basis set level of theory was adopted to calculate the properties of the title molecule. All the theoretical calcu-

Table 1
Calculated optimized parameter values of the ACMP [Bond length in (Å), angles in (°)].

Bond lengths	B3LYP	Exp.[a]	Bond angles	B3LYP	Exp.[a]	Dihedral angles	B3LYP	Exp.[a]
N1—C2	1.344	1.358	C2—N1—C6	116.2	115.9	C6—N1—C2—N3	0.0	0.6
N1—C6	1.323	1.320	N1—C2—N3	126.1	125.4	C6—N1—C2—N9	−180.0	−179.6
C2—N3	1.340	1.354	N1—C2—N9	117.0	117.3	C2—N1—C6—C5	0.0	−1.6
C2—N9	1.354	1.338	N3—C2—N9	116.9	117.3	C2—N1—C6—O12	180.0	178.6
N3—C4	1.320	1.327	C2—N3—C4	115.4	114.9	N1—C2—N3—C4	0.0	0.2
C4—C5	1.380	1.374	N3—C4—C5	124.9	126.1	N9—C2—N3—C4	180.0	−179.6
C4—Cl8	1.755	1.745	N3—C4—Cl8	116.2	114.9	N1—C2—N9—H10	−0.2	
C5—C6	1.403	1.403	C5—C4—Cl8	118.9	118.9	N1—C2—N9—H11	−179.8	
C5—H7	1.077	0.950	C4—C5—C6	114.3	113.3	N3—C2—N9—H10	179.8	
C6—O12	1.338	1.348	C4—C5—H7	123.7	123.4	N3—C2—N9—H11	0.2	
N9—H10	1.004	0.828	C6—C5—H7	122.0	123.4	C2—N3—C4—C5	0.0	−0.2
N9—H11	1.004	0.850	N1—C6—C5	123.2	124.5	C2—N3—C4—Cl8	−180.0	−179.4
O12—C13	1.433	1.439	N1—C6—O12	119.7	119.5	N3—C4—C5—C6	0.0	−0.6
C13—H14	1.090	0.980	C5—C6—O12	117.1	116.0	N3—C4—C5—H7	−180.0	
C13—H15	1.087	0.980	C2—N9—H10	119.8	119.1	Cl8—C4—C5—C6	−180.0	178.5
C13—H16	1.090	0.980	C2—N9—H11	119.4	118.7	Cl8—C4—C5—H7	0.0	
			H10—N9—H11	120.9	122.1	C4—C5—C6—N1	0.0	1.6
			C6—O12—C13	118.2	117.4	C4—C5—C6—O12	180.0	−178.6
			O12—C13—H14	110.8	109.5	H7—C5—C6—N1	180.0	
			O12—C13—H15	105.1	109.5	H7—C5—C6—O12	0.0	
			O12—C13—H16	110.8	109.5	N1—C6—O12—C13	0.0	−0.7
			H14—C13—H15	110.5	109.5	C5—C6—O12—C13	180.0	179.4
			H14—C13—H16	109.1	109.5	C6—O12—C13—H14	60.6	
			H15—C13—H16	110.5	109.5	C6—O12—C13—H15	−180.0	
						C6—O12—C13—H16	−60.6	

[a] Taken from [15].

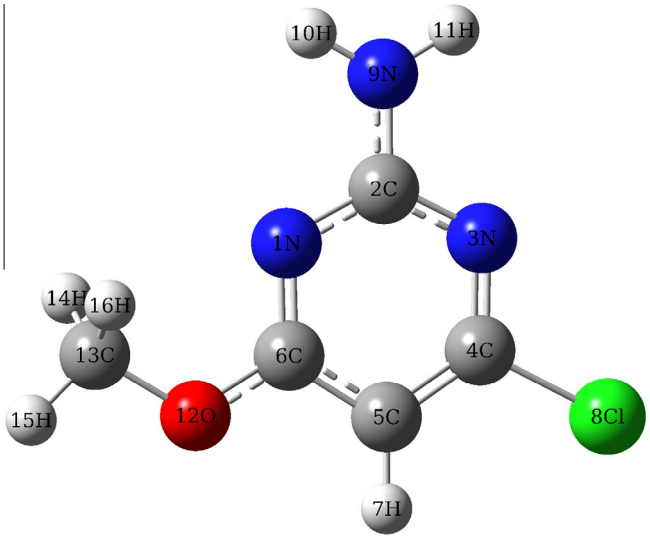

Fig. 3. Optimized Molecular structure and atomic numbering of ACMP.

lations were performed using the Gaussian 03W program package [8] with the default convergence criteria, without any constraint on the geometry [9]. The equilibrium geometry corresponding to the true minimum on the potential energy surface (PES) was effectively obtained by solving self-consistent field equation. The vibrational spectra of the ACMP were obtained by taking the second derivative of energy, computed analytically. The optimized structural parameters were used in the vibrational frequency calculations at DFT level to characterize all stationary points as minima using the GAUSSVIEW animation program [10]. Vibrational frequencies were computed at DFT level which had reliable one-to-one correspondence to experimental IR and Raman frequencies [11]. In the present study we have used the following scaling factor of 0.983 and 0.958 [12] for B3LYP/6-311++G(df,pd) method. A comparison of the calculated frequencies with the experimental values revealed that the 6-311++G(df,pd) basis set result shows very good agreement with the experimental observations.

Prediction of Raman intensities

The Raman activities (S_{Ra}) calculated with Gaussian 03 program [8] converted to relative Raman intensities (I_{Ra}) using the following relationship derived from the intensity theory of Raman scattering [13,14]

$$I_i = \frac{f(v_0 - v_i)^4 S_i}{v_i[1 - \exp(-hcv_i/kt)]}$$

where v_0 is the laser exciting wavenumber in cm^{-1} (in this work, we have used the excitation wavenumber v_0 = 9398.5 cm^{-1}, which corresponds to the wavelength of 1064 nm of a Nd-YAG laser), v_i the vibrational wavenumber of the ith normal mode (cm^{-1}) while S_i is the Raman scattering activity of the normal mode v_i. f (is a constant equal to 10^{-12}) is a suitably chosen common normalization factor for all peak intensities. h, k, c and T are Planck and Boltzmann constants, speed of light and temperature in Kelvin, respectively. For the simulation of calculated FT-Raman spectra have been plotted using pure Lorentzian band shape with a bandwidth of Full Width at Half Maximum (FWHM) of 10 cm^{-1}.

Results and discussion

Molecular geometry

The optimized parameters namely, bond lengths and angles of ACMP calculated by DFT/B3LYP method with the 6-311++G(df,pd) basis set are listed in Table 1 and are in accordance with atom numbering scheme given in Fig. 3. The investigation and interpretation were performed depending on the exact crystal structure of the title molecule available in the literature [15] and theoretically obtained results. As a result of experimental findings and our calculations, the amino substituted position of N1—C2 (1.344 Å) and C2—N3 (1.340 Å) bond length values are higher than the ring C—N bond length values which are fall in 1.323 Å, 1.320 Å for N1—C6 and N3—C4. The X-ray diffraction data also well in agreement with the above calculated values which are (1.358/1.354 Å) and (1.320/1.327 Å) in both the cases. In accordance to the methyl

Table 2
Comparison of the experimental and calculated vibrational spectra and proposed assignments of ACMP.

No	FT-IR	FT-Raman	Unscaled	Scaled	I_{IR}	SA_{Raman}	I_{Raman}	Assignments (TED)
1	3450	3452	3767	3609	64.24	45.73	0.01	υ_{asym} NH_2 (100)
2	3324		3631	3479	105.51	162.15	0.03	υ_{sym} NH_2 (100)
3	3200	3183	3250	3113	2.17	77.89	0.02	υ CH (99)
	3103	3094						Overtone combination
	3030	3032						Overtone combination
4	3004	3005	3150	3018	16.49	100.98	0.04	υ_{asym} CH_3 (100)
5	2954	2958	3118	2987	19.98	46.17	0.02	υ_{asym} CH_2 of CH_3 (100)
6	2899	2897	3045	2917	40.53	177.93	0.07	υ_{sym}. CH_3 (100)
7	1655	1650	1637	1609	709.66	13.90	0.04	ρ NH_2 (56) + υ C—NH_2 (20)
8	1594	1598	1614	1586	261.34	17.35	0.05	υ C—N (51) + υ CC_{ring} (19) + ρ NH_2 (13)
9	1558	1568	1585	1558	591.27	0.70	0.00	υ C—N (40) + υ CC_{ring} (24)
10	1507	1515	1509	1484	46.07	1.55	0.01	CH_3 umbrella (37) + υ C—O (15) + υ C—N (13)
11	1465	1464	1499	1473	18.98	5.73	0.02	ρ CH_2 of CH_3 (94)
12			1484	1459	8.98	13.19	0.05	ρ CH_2 of CH_3 (61) + β CH of CH_3 (39)
13	1449	1451	1474	1449	110.68	3.15	0.01	υ C—NH_2 (28) + CH_3 umbrella (15) + υ C—N (14) + ρ NH_2 (14)
14	1400	1403	1436	1412	125.68	2.89	0.01	CH_3 umbrella (31) + υ C—N (23) + β CH (20)
15	1334	1341	1367	1343	186.16	7.23	0.04	υ C—C (25) + υ C—O (25) + υ C—N (18)
16	1253	1259	1296	1274	44.62	5.90	0.03	Ring Deformation (87)
17	1201	1202	1221	1200	67.04	2.67	0.02	r CH_3 (75)
18	1161	1162	1171	1151	0.66	3.07	0.02	t CH_2 of CH_3 (98)
19			1163	1143	83.74	3.08	0.02	β CH (47) + r NH_2 (13) + υ C—C (12)
20	1103	1103	1116	1097	47.91	0.24	0.00	r NH_2 (17) + υ CN (10) + υ CO (13) + υ O—CH_3 (12) + β CH of CH_3 (12) + υ C—C (10)
21	1040	1043	1039	1021	52.42	3.42	0.03	υ O—CH_3 (47) + r NH_2 (20)
22	1003	1003	1016	999	99.07	1.88	0.02	r NH_2 (26) + β CCC_{ring} (21) + υ CN (13) + υ O—CH_3 (12)
23	970	971	986	969	4.98	23.18	0.26	υ CN (49) + β (CCN + NCN) (21) + υ CC_{ring} (12)
24	862	870	871	856	67.43	3.33	0.05	υ C—Cl (24) + υ O—CH_3 (14) + β (CCN + NCN) (14) + υ C—O (10)
25	802	803	820	806	45.58	0.60	0.01	γ CH (57) + γ (CCCN + CNCN) (30)
26	776		797	784	0.38	0.04	0.00	γ CNCN (63) + γ CH (30)
27	686	704	704	692	0.92	0.54	0.01	γ CNCC (45) + γ CH (32)
28	649	647	644	633	3.73	2.67	0.08	β CCN (44) + β COC (28)
29		624	642	631	1.29	0.15	0.00	γ CCCCl (82)
30	605	601	610	600	2.40	9.89	0.34	β (CCN + NCN) (72) + υ C—N (13)
31	519	522	538	529	0.15	0.16	0.01	t NH_2 (99)
32			509	500	3.16	3.10	0.16	β (CCN + NCN) (53) + r NH_2 (34)
33	463	455	445	437	3.30	2.28	0.16	β (CCN + NCN) (35) + υ C—Cl (27) + r NH_2 (14) + β COC (14)
34		375	362	356	14.88	9.12	1.00	υ C—Cl (31) + r NH_2 (19) + β COC (18)
35		283	252	248	0.49	2.91	0.01	β CC—Cl (50) + r NH_2 (19) + β COC (13)
36		250	242	238	1.33	0.36	0.00	γ CCNC (44) + τ CH_3 (22) + γ CCOC (21)
37		212	198	195	37.90	0.26	0.00	Ring butterfly (98)
38			197	194	1.90	0.84	0.00	β CCO (43) + β COC (24) + β CCl (21)
39			189	186	0.17	0.25	0.00	γ (CCCN + CCNC) (73)
40		149	161	158	1.59	0.71	0.00	τ CH_3 (89)
41		72	90	89	2.09	0.17	0.00	γ O—CH_3 (70)
42		59	67	66	194.53	0.01	0.00	τ NH_2 (90)

υ_{sym} – υ_{asym}; symmetric–asymmetric stretching, β; in plane bending, γ; out of plane bending, ρ; scissoring, ω; wagging, t; twisting, r; rocking, τ; torsion. [frequency (cm^{-1}); I_{IR} (K $mmol^{-1}$), IR intensity; SA_{Raman} ($Å^4$ amu^{-1}), Raman scattering activities; I_{Raman} (Arb. units) Raman intensities. The out-of-plane bonded atoms were underlined in the last column.]

substitution, the methyl connected C—O (1.433 Å/1.439 Å) bond length increased maximum compare to the pyrimidine connected C—O (1.338 Å/1.348 Å) bond length, the experimental results also agree well. The bond lengths C5—C6 (1.403 Å) and N1—C6 (1.323 Å) affected by electronegativity atom substitution because which are differ from the values 1.397 and 1.338 Å [7] respectively. The bond angles calculated by DFT (B3LYP) method are nearly equal to the experimental values. The endocyclic bond angle C5—C6—N1, N1—C2—N3, N3—C4—C5 and C4—C5—C6 values are calculated with maximum deviation at 123.2°, 126.1°, 124.9° and 114.3° which are observed in experimental X-ray data at 124.5°, 125.4°, 126.1° and 113.3° respectively which may be the reason of the amino and methoxy substitutions and also intermolecular hydrogen bonding interaction. The dihedral angles C5—C6—O12—C13 (180°), N1—C6—O12—C13 (0°) and N1—C2—N9—H10 (179.8°), N1—C2—N9—H11 (179.8°) show the planarity of the entire molecule. As seen from Table 1, the optimized parameters are slightly overestimated from the experimental values due to the fact that the experimental results belong to the solid phase and theoretical calculations belong to isolated molecule in gas phase.

Vibrational assignments

We performed a frequency calculations analysis to obtain the spectroscopic signature of ACMP in this study. The recorded FT-IR, FT-Raman and the calculated vibrational wavenumbers, along with their relative intensities and probable assignments, are given in Table 2. The title molecule consists of 16 atoms, which has 42 vibrational degrees of freedom. The 42 normal modes of ACMP have been assigned according to the detailed vibrations of the individual atoms. The molecule under investigation was assumed to possess C1 point group symmetry. The vibrational assignments have been made based on the Gaussview animation package [10] along with available related molecules in the literature. A complete assignment of the fundamentals was also proposed based on the calculated TED values, infrared and Raman intensities. The calculated wavenumbers were usually higher than the corresponding experimental quantities, due to the combination of electron correlation effects and basis set deficiencies. After applying, the scaling factor of the DFT/B3LYP/6-311++G(df,pd) level of theory, the theoretical wavenumbers were found to be in good agreement with the experimental wavenumbers.

Table 3
The observed (in DMSO) and predicted ^{1}H and ^{13}C NMR isotropic chemical shifts (with respect to TMS, all values in ppm) for ACMP.

Atom	Experimental	6-311++G(df,pd)		Atom	Experimental	6-311++G(df,pd)	
	DMSO	Gas	DMSO		DMSO	Gas	DMSO
H7	7.05	5.78	5.83	C2	160.3	161.0	162.5
H10	6.09	4.22	4.71	C4	163.4	171.0	170.3
H11	6.09	4.32	4.68	C5	94.6	95.9	96.2
H14	3.82	3.53	3.60	C6	171.4	172.3	173.8
H15	3.82	3.37	3.56	C13	54.1	50.6	51.9
H16	3.82	3.53	3.60				

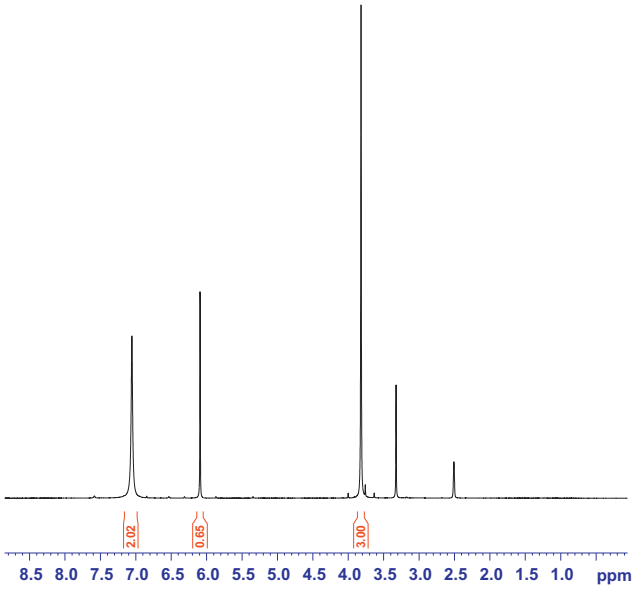

Fig. 4. ^{1}H NMR spectrum of ACMP.

NH_2 vibrations

In all the primary aromatic amines, the N—H stretching wavenumbers occur in the region 3300–3500 cm^{-1}. The NH_2 group gave rise to six internal modes of vibrations such as the asymmetric stretching (υ_{as}), symmetric stretching (υ_s), the symmetric planar deformation or scissoring (δ_s), the anti-symmetric planar deformation or rocking (δ_{as}), the symmetric non-planar deformation or wagging (ω) and the anti-symmetric non-planar deformation or torsion (τ). The molecule under investigation possesses one NH_2 group and hence one expects one asymmetric and one symmetric N—H stretching vibrations. The NH_2 asymmetric and symmetric stretching vibration in FT-IR spectrum found at 3414 cm^{-1} and 3312 cm^{-1}, respectively for 2-amino-4,6-dimethoxy pyrimidine molecule [16].

The scaled NH_2 asymmetric and symmetric stretching modes were at 3609 and 3479 cm^{-1} (mode Nos. 1 and 2) by B3LYP/6-311++G(df,pd) level of theory. The observed experimental FT-IR spectrum showed two bands at 3450 and 3324 cm^{-1} with little deviation which might be due to the intermolecular hydrogen bonding between hydrogen atom of amino group and the oxygen atom of methoxy group. As expected these modes are pure stretching modes as it is evident from TED column, they are exactly contributing to 100%. Bellamy et al. [17,18] have suggested that the NH_2 scissoring mode lies in the region 1529–1650 cm^{-1}. Baran et al. [16] have reported the NH_2 scissoring at 1680 cm^{-1} (IR), 1694 cm^{-1} (Raman) and 1664 cm^{-1} (IR), 1695 cm^{-1} (Raman) for metal complexes of L-asparagine and L-glutamic acid 5-amide respectively. In accordance with the above literature data, in our present study the NH_2 scissoring frequency was found at 1609 cm^{-1} by B3LYP method is matching with medium FT-Raman band at 1650 cm^{-1} and FT-IR spectra at 1655 cm^{-1}. The NH_2 rocking mode predicted at 1021 and 999 cm^{-1} by B3LYP method showed good agreement with the recorded value of 1040, 1003 and 1043, 1003 cm^{-1} in the FT-IR and FT-Raman spectra respectively.

C—H vibrations

The assignments of the benzene ring vibrations are relatively easy because these vibrations are observed at very similar wavenumbers in different compounds. The respective bands appear in the whole range of the spectrum [19]. In the ACMP molecule, only one C—H stretching vibration was assigned which was represented as mode No. 3 for the pyrimidine ring. The C—H stretching vibration in FT-IR and FT-Raman spectrum is observed at 3198 and 3192 cm^{-1} respectively for 2-amino-4-chloro-6-methylpyrimidine [7]. The very strong band is observed in FT-IR at 3200 cm^{-1} and a weak FT-Raman band at 3183 cm^{-1} is assigned as C—H stretching vibration. The harmonic frequencies by B3LYP/6-311++G(df,pd) level of theory predicted at 3113 cm^{-1} fall within the recorded spectral range. As expected these modes are pure stretching modes as it is evident from TED column, they are exactly contributing to 99%.

The aromatic C—H bending vibration occurs in the region 1400–1000 cm^{-1}, the bands are sharp but are weak to medium intensity. The C—H in-plane bending harmonic vibrations computed at 1412 and 1143 cm^{-1} by B3LYP method show excellent agreement with medium and strong FT-IR band at 1400 cm^{-1} and FT-Raman bands at 1403 cm^{-1} are assigned to C—H in-plane bending vibrations. The literature values at 1434 and 1436 cm^{-1} in FT-IR and FT-Raman spectrum respectively show in good agreement [7]. The TED corresponds to this mode are mixed modes as it is evident from Table 2.

—OCH_3 vibrations

The asymmetric C—H stretching mode of CH_3 group is expected around 2980 cm^{-1} and the symmetric [20,21] one is expected in the region 2870 cm^{-1}. Electronic effects such as back-donation and induction, mainly caused by the presence of oxygen atom adjacent to CH_3 group, can shift the position of CH stretching and bending modes [22–25]. Vibrational spectral studies on esters have shown that asymmetric and symmetric methyl stretching bands can be observed around 2960 and 2846 cm^{-1}, respectively [26,27]. In accordance with the above literature data, in the present case the asymmetric stretching modes of CH_3 group are observed in IR spectrum at 3004 and 2954 cm^{-1} the symmetric stretching vibration is observed in IR at 2899 cm^{-1}. The Raman bands observed at 3005 and 2958 cm^{-1} correspond to the asymmetric and the band at 2897 cm^{-1} to the symmetric CH_3 stretching modes. The asymmetric and symmetric stretching modes of CH_3 group are calculated to be 3018, 2987 and 2917 cm^{-1}, respectively. As expected these modes are pure stretching modes as it is evident from TED column, they are exactly contributing to 100%. The lowering of this mode for CH_3 is probably due to its proximity to the pyrimidine ring. The CH_3 umbrella modes are also found in the expected

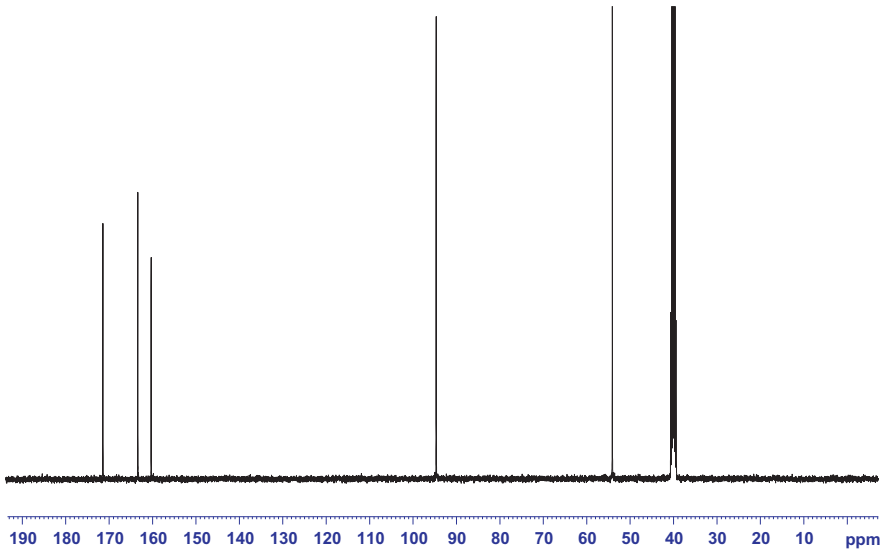

Fig. 5. ^{13}C NMR spectrum of ACMP.

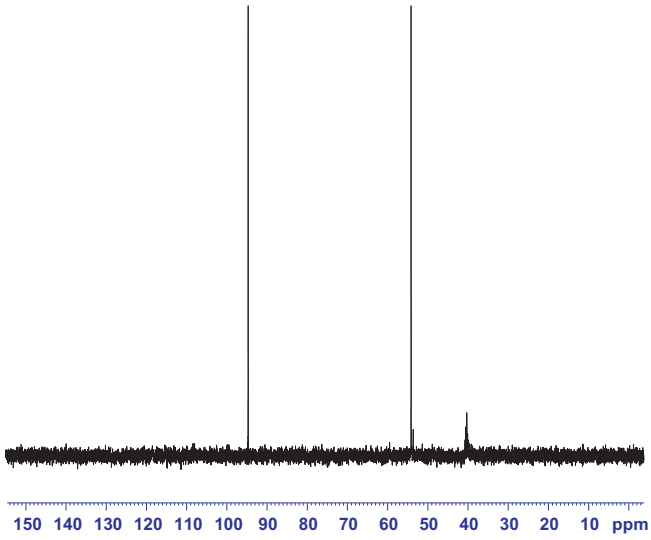

Fig. 6. DEPT 135 NMR spectrum of ACMP.

range: 1507, 1449 and 1400 cm^{-1} in FT-IR and 1515, 1451 and 1403 cm^{-1} in FT-Raman can also be supported by the computation. The rocking vibrations of the CH_3 in ACMP is observed at 1201 and 1202 cm^{-1} for CH_3 rocking in FT-IR and FT-Raman spectrum respectively correlated well with the calculated values at 1200 cm^{-1}. As expected these modes are pure rocking modes as it is evident from TED column, they are exactly contributing to 75%.

C—Cl vibrations

C—Cl absorption is observed in the broad region between 850 and 550 cm^{-1}. The vibrations belonging to the bond between the ring and the halogen atoms are worth to discuss here, since mixing of the vibration is possible due to the lowering of the molecular symmetry and the presence of heavy atom on the periphery of molecule [28]. Mooney [29,30] assigned vibrations of C—X group (X = Cl, Br and I) in the frequency range 1129–480 cm^{-1}.We have assigned C—Cl stretching vibration by theoretically at 856 cm^{-1} for B3LYP/6-311++G(df,pd) level of theory. The observed bands are appeared at 862 and 870 cm^{-1} FT-IR and FT-Raman spectra respectively which correlates well with the calculated one. Furthermore, the C—Cl deformation vibrations are observed at 624 cm^{-1} in FT-Raman spectrum. The theoretically calculated wavenumbers at 631 cm^{-1} show good agreement with experimental data.

C—O—C vibrations

The (O—C) and (C—O) stretching vibrations have already been reported by Druzbicki et al. [31] Dolega et al. [32] and Vijaya Chamundeeswari et al. [33] at ca. 1270 cm^{-1} and ca. 1040 cm^{-1}. In the present study, we have calculated the ν(O-Cpyrimidine) frequency in methoxypyrimidine group at 1343 cm^{-1}. On the otherhand, the stretching vibrations of the ν(Cmethyl-O) bond assigned at 1021 cm^{-1}. The observed bands are appeared at 1334, 1040 and 1341, 1043 cm^{-1} in FT-IR and FT-Raman spectra respectively show good agreement with theoretically calculated wavenumbers.

Ring vibrations

For the parasubstituted benzene ring, the C—C ring stretching modes are observed at 1590, 1474, 1395, 1308 and 1232 cm^{-1} (IR), 1599, 1574, 1489, 1406 and 1310 cm^{-1} (Raman) an 1589, 1578, 1478, 1384, 1300 and 1229 cm^{-1} theoretically [26,27]. The C—C ring stretching mode of ACMP appears in our calculations at 1558 cm^{-1} and it contributes 24% TED with major contribution of 51% υCN. The other C—C ring stretching mode appears at higher frequency of 1586 cm^{-1} with 19% TED contribution. The TED of these assignments predicts that they are mixed modes with some contribution of υC—N vibration. Primary aromatic amines with nitrogen directly on the ring absorb at 1330–1260 cm^{-1} due to stretching of the phenyl carbon nitrogen bond [34,26]. The theoretically computed values of C—N and C=N stretching vibrations are found in the range 1457–1558 cm^{-1}. For our title molecule, the DFT calculations give the υC—N mode at 1586, 1558, 1449 and 969 cm^{-1} and at 1594, 1558, 1449 and 970 cm^{-1} in FT-IR spectrum and 1598, 1568, 1451 and 971 cm^{-1} in FT-Raman spectrum. In our calculations, this mode is a mixed mode as it is evident from TED calculations.

^{1}H and ^{13}C NMR analysis

The calculated values of ^{13}C and ^{1}H chemical shifts by B3LYP/6-311++G(df,pd) level of theory in DMSO environment are summa-

Table 4
The experimental and computed absorption wavelength λ (nm), excitation energies E (eV), absorbance and oscillator strengths (f) of ACMP in ethanol and water solution and gas phase.

Experimental			TD-B3LYP/6-311++G(df,pd)			CIS/6-311++G(df,pd)		
λ (nm)	E (eV)	Abs.	λ (nm)	E (eV)	f	λ (nm)	E (eV)	f
Ethanol								
278.0	4.4964	0.664	256.71 (41 → 42)	4.8298	0.1282	206.77 (41 → 49)	5.9962	0.3814
232.5	5.3763	0.771	233.30 (40 → 42)	5.3145	0.0035	186.17 (41 → 42)	6.6598	0.0215
			219.72 (41 → 44)	5.6428	0.0130	183.59 (41 → 52)	6.7534	0.4470
Water								
277.5	4.5045	0.392	256.80 (41 → 42)	4.8281	0.1260	206.49 (41 → 49)	6.0043	0.3732
229.5	5.4466	0.781	233.17 (40 → 42)	5.3173	0.0035	186.05 (41 → 42)	6.6641	0.0210
			219.51 (41 → 44)	5.6483	0.0128	183.25 (41 → 52)	6.7660	0.4356
Gas								
			250.67 (41 → 42)	4.9460	0.1012			
			234.99 (40 → 42)	5.2761	0.0021			
			227.91 (41 → 44)	5.4401	0.0117			

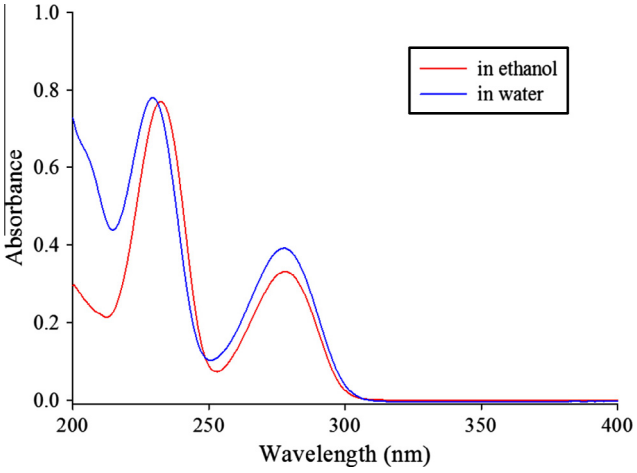

Fig. 7. Comparison of experimental UV–Vis spectrum (ethanol and water) of ACMP.

rized for the ACMP in Table 3. DFT shielding calculations are rapid and applicable to large systems, but the paramagnetic contribution to the shielding tends to be overestimated. In this sense, theoretical calculations of the chemical shifts may be used as an aid for the assignment of the experimental data and for the study of our title molecule. The observed ^{1}H, ^{13}C and DEPT NMR spectra of the ACMP molecule are given in the Figs. 4–6, respectively. The experimental values are also included in the Table 3. It is noted that the maximum deviation from experimental chemical shift for ^{13}C NMR chemical shift is 6.9 ppm (C4 atom) and the ^{1}H chemical shift, the maximum deviation from experimental value is 1.41 ppm (H11) in DMSO solution. The cumulative influence of oxygen atom (O12) and methyl substitution lead reduced the electron density of the carbon atom C6, thus its NMR signal is observed in the very downfield at 171.4 ppm. As can be seen from Table 3, there is a good agreement between experimental and theoretical chemical shift results for the title compound. Aromatic carbons give signals in overlapped areas of the spectrum with chemical shift values from 100 to 150 ppm [35,36]. As per the literature results, the C5 NMR signal is observed in the shielding region at 94.6 ppm. Due to the electron withdrawing environmental, the H10 and H11 chemical shifts are observed in the shielded region at 6.09 ppm appear as singlet peak. In our present investigation, the experimental chemical shift values of aromatic carbons are in the range 94.6–171.4 ppm. As can be seen from Table 3, the calculated values show moderate agreement with measured values. The minimum of deviation may be due to the influence of rapid proton exchange, hydrogen bond and solvent effect.

Absorption spectra

On the basis of the fully optimized ground-state structure, TD-DFT/B3LYP/6-311++G(df,pd) calculations have been performed to determine the low-lying excited states of ACMP. The calculated result involving the vertical excitation energies, oscillation strength (f) and wavelength were carried out and compared with the measured experimental wavelength listed in Table 4. Typically, according to the Frank–Condon principle, the maximum absorption peak λ_{max} corresponds in an UV–Vis spectrum to vertical excitation. TD-DFT/B3LYP/6-311++G(df,pd) level of theory predicts two intense electronic transition at 4.8298/5.3145 eV (256.71/233.30 nm) with oscillator strength f = 0.1282/0.0035 for ethanol and 4.8281/5.3173 eV (256.80/233.17 nm) with oscillator strength f = 0.1260/0.0035 for water in good agreement with the measured experimental data in ethanol and water solutions (exp = 278.0/232.5 nm and 277.5/229.5 nm) respectively as shown in Fig. 7. The calculated UV spectrum (Gas phase, Ethanol and Water) of ACMP by TD-B3LYP/6-311++G(df,pd) and CIS/6-311++G(df,pd) level of theory are shown in Supplementary data S1 and S2 respectively. All the structures allowed strong π–π^* and σ–σ^* transition in the UV–Vis region with high extinction coefficients. The π–π^* transitions were expected to occur relatively at lower wavelengths, due to the consequence of the extended aromaticity of the pyrimidine ring. The above electronic transitions were mainly derived from the contribution of π–π^* bands.

Frontier molecular orbital analysis

Both the highest occupied molecular orbital (HOMO) and lowest unoccupied molecular orbital (LUMO) are the main orbital take

Table 5
Frontier molecular orbital energies (eV) and dipol moment (μ, in Debye) of ACMP.

Parameters	TD-B3LYP/6-311++G(df,pd)			CIS/6-311++G(df,pd)		
	Gas	Ethanol	Water	Parameters	Ethanol	Water
E_{total}	−24327.3881	−24327.6046	−24327.6145	E_{total} (eV)	−24237.6919	−24237.7027
E_{LUMO+2}	−0.4079	−0.2316	−0.2291	$E_{LUMO+10}$	3.1993	3.1936
E_{LUMO}	−0.9557	−1.1113	−1.1192	E_{LUMO+7}	2.6591	2.6515
E_{HOMO}	−6.5879	−6.6541	−6.6584	E_{LUMO}	1.1249	1.1290
E_{HOMO-1}	−7.5831	−62.1951	−7.7822	E_{HOMO}	−9.2495	−9.2549
$\Delta E_{(LUMO+2)-HOMO}$	6.1800	6.4225	6.4293	$\Delta E_{(LUMO+10)-HOMO}$	12.4488	12.4485
$\Delta E_{LUMO-HOMO}$	5.6323	5.5427	5.5392	$\Delta E_{(LUMO+7)-HOMO}$	11.9086	11.9064
$\Delta E_{LUMO-(HOMO-1)}$	6.6274	61.0838	6.6630	$\Delta E_{LUMO-HOMO}$	10.3744	10.3839
μ_x	3.2882	4.0916	4.1283	μ_x	4.0463	4.0778
μ_y	1.5676	1.8210	1.8267	μ_y	1.6843	1.6865
μ_z	0.0080	0.0099	0.0100	μ_z	0.0106	0.0107
μ_{tot}	3.6428	4.4785	4.5144	μ_{tot}	4.3829	4.4128

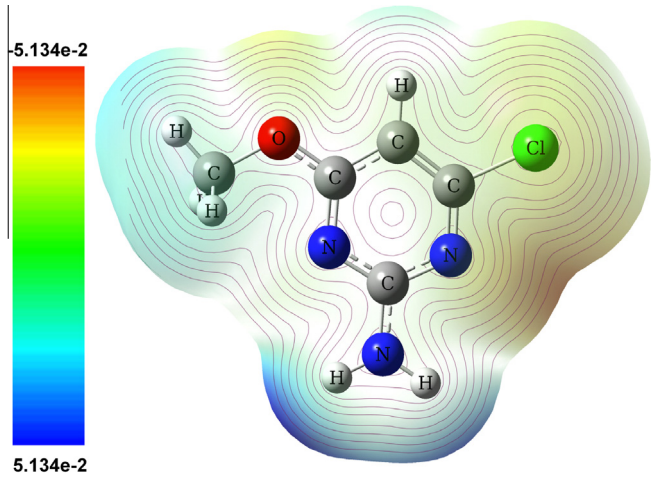

Fig. 8. Molecular electrostatic potential map of ACMP calculated by B3LYP/6-311++G(df,pd) method.

part in chemical stability [37]. The HOMO represents the ability to donate an electron, LUMO as an electron acceptor represents the ability to obtain an electron. The HOMO and LUMO energy calculated by B3LYP/6-31+G(d,p) method as shown below. This electronic absorption corresponds to the transition from the ground to the first excited state and is mainly described by one electron excitation from the highest occupied molecular orbital (HOMO) to the lowest unoccupied molecular orbital (LUMO). The HOMO is located over the pyrimidine, the HOMO → LUMO transition implies an electron density transfer within the ring. Moreover, these orbital significantly overlap in their position for ACMP. The energy values and atomic orbital compositions of the frontier molecular orbital are shown in Table 5 and Supplementary data S3 respectively

HOMO energy = −6.5879 eV
LUMO energy = −0.9557 eV
HOMO−LUMO energy
gap = 5.6323 eV

Molecular electrostatic potential (MEP)

Molecular electrostatic potential (MEP) generally present in the space around the molecule by the charge distribution is very useful in understanding the sites of electrophilic attacks and nucleopilic reaction for the study of biological recognition process [38] and hydrogen bonding interactions [39]. In order to predict the molecular reactive sites, the MEP for our title molecule is calculated by B3LYP/6-311++G(df,pd) method as shown in Fig. 8. The different values of the electrostatic potential at the surface are represented by different colors. Potential increases in the order red < orange < yellow < green < blue. The color code of these maps is in the range between −32.2163 kcal mol^{-1} (deepest red) and 32.2163 kcal mol^{-1} (deepest blue) in compound, where blue indicates the strongest attraction and red indicates the strongest repulsion. As can be seen from the MEP map of the title molecule, while regions having the negative potential are over the electronegative atom (oxygen and nitrogen atoms), the regions having the positive potential are over the hydrogen atoms. From these results, we can say that the H atoms indicate the strongest attraction and O atom indicates the strongest repulsion.

Conclusion

In the study, we have investigated to clarify the characterization of ACMP by using of computational methods. The FT-IR and FT-Raman spectra of ACMP were studied. The molecular geometry and wavenumber have been calculated using DFT/B3LYP with 6-311++G(df,pd) basis set and the normal modes are assigned based on TED values. From the optimized geometry results, we can conclude that the ACMP molecule is highly conjugated and π electron delocalized. The ^{1}H and ^{13}C NMR chemical shifts have been calculated and compared with the experimental one. All the data have been compared with experimental values and shown to have a good agreement with each other. The UV spectrum was measured in water and ethanol solutions. HUMO and LUMO orbitals have been visualized. It has been conclude that the lowest singlet excited state of the ACMP molecule is mainly derived from the HOMO → LUMO ($\pi \rightarrow \pi^*$) electron transition. The MEP map shows that the negative potential sites are on electronegative atoms while the positive potential sites are around the hydrogen atoms.

Appendix A. Supplementary material

Supplementary data associated with this article can be found, in the online version, at http://dx.doi.org/10.1016/j.saa.2013.07.044.

References

[1] I.M. Lagoja, Chem. Biodiv. 2 (1) (2005) 1–50.
[2] H.K.S. Souza, Thermochim. Acta 501 (2010) 1–7.
[3] F. Hueso, N.A. Illan, M.N. Moreno, J.M. Martinez, M.J. Ramirez, J. Inorg. Biochem. 94 (2003) 326–334.
[4] D.A. Ibrahim, A.M. El-Metwally, Eur. J. Med. Chem. 45 (2010) 1158–1166.
[5] T. Eicher, S. Hauptmann, The Chemistry of Heterocycles, second ed., Wiley-VCH, Weinheim, 2003.
[6] M. Mogren, K. Al-Farhan, A.A. Hasanein, J. Sau. Chem. Soc. 17 (2013) 87–95.
[7] T. Jayavarthanan, N. Sundaraganesan, M. Karabacak, M. Cinar, M. Kurt Spectrochim, Acta Part A 97 (2012) 811–824.

[8] Gaussian 03 program, (Gaussian Inc, Wallingford CT), 2004.
[9] H.B. Schlegel, J. Comp. Chem. 3 (1982) 214–218.
[10] A. Frisch, A.B. Nielson, A.J. Holder, GAUSSVIEW User Manual, Gaussian Inc, Pittsburgh, PA, 2000.
[11] V. Krishnakumar, R. Mathammal, S. Muthunatesan, Spectrochim. Acta 70A (2008) 210–216.
[12] P.M. Wojciechowski, W. Zierkiewicz, D. Michalska, J. Chem. Phys. 118 (24) (2003) 10900–10911.
[13] G. Kereztury, S. Holly, J. Varga, G. Besenyei, A.Y. Wang, J.R. Durig, Specrochim. Acta 49A (2007) (1993) 2019.
[14] G. Kereztury, in: J.M. Chalmers, P.R. Griffith (Eds.), Raman Spectroscopy: Theory, in Hand book of Vibrational Spectroscopy, 1, John Wiley & Sons Ltd, New York, 2002.
[15] K. Thanigaimani, N.C. Khalib, S. Arshad, I.A. Razak, Acta Cryst. E68 (2012) o3318.
[16] N. Sundaraganesan, K. Satheshkumar, C. Meganathan, B.D. Joshua, Spectrochim. Acta 65A (2006) 1186–1196.
[17] L.J. Bellamy, R.L. Williams, Spectrochim. Acta 9 (1957) 341–345.
[18] L.J. Bellamy, The Infrared Spectra of Complex molecules, 2, Chapman and Hall, London, 1980.
[19] G. Varsanyi, Vibrational Spectra of Benzene Derivatives, Academic Press, New York, 1969.
[20] D. Sajan, I. Hubert Joe, V.S. Jayakumar, J. Raman Spectrosc. 37 (2005) 508–519.
[21] M. Gussoni, C. Castiglioni, M.N. Ramos, M.C. Rui, G. Zerbi, J. Mol. Struct. 224 (1990) 445–470.
[22] B. Smith, Infrared Spectral Interpretation, A Systematic Approach, CRC Press, Washington, DC, 1999.
[23] M. Gussoni, C. Castiglioni, J. Mol. Struct. 521 (2000) 1–3.
[24] J. Palomar, J.L.G. De Paz, J. Catalan, Chem. Phys. 246 (1999) 167–208.
[25] M. Rumi, G. Zerbi, J. Mol. Struct. 509 (1999) 11–28.
[26] N.B. Colthup, L.H. Daly, S.E. Wiberley, Introduction to Infrared and Raman Spectroscopy, Academic Press, New York, 1990.
[27] G. Socrates, Infrared Characteristic Group Frequencies, Wiley-Interscience Publication, 1980.
[28] R.A. Yadaav, I.S. Singh, Indian J. Pure Appl. Phys. 23 (1985) 626–627.
[29] E.F. Mooney, Spectrochim. Acta 20 (1964) 1021–1032.
[30] E.F. Mooney, Spectrochim. Acta 19 (1963) 877–887.
[31] K. Druzbicki, E. Mikuli, M.D.O. Chrusciel, Vib. Spectro. 52 (2010) 54–62.
[32] D. Dolega, A.M. Mikuli, J. Chrusciel, J. Mol. Struct. 933 (2009) 30–37.
[33] S.P.V. Chamundeeswari, E.J.J. Samuel, N. Sundaraganesan Spectrochim, Acta Part A 110 (2013) 36–45.
[34] H. Arslan, U. Florke, N. Kulcu, G. Binzet, Spectrochim. Acta 68A (2007) 1347–1355.
[35] H.O. Kalinowski, S. Berger, S. Braun, Carbon-13 NMR Spectroscopy, John Wiley & Sons, Chichester, 1988.
[36] K. Pihlaja, E. Kleinpeter (Eds.), Carbon-13 Chemical Shifts in Structural and Sterochemical Analysis, VCH Publishers, Deerfield Beach, 1994.
[37] S. Gunasekaran, R.A. Balaji, S. Kumeresan, G. Anand, S. Srinivasan, Can. J. Anal. Sci. Spectrosc. 53 (2008) 149–162.
[38] P. Politzer, P.R. Laurence, K. Jayasuriya, Health Persp. 61 (1985) 191–202.
[39] P. Politzer, P. Lane, Struct. Chem. 61 (1990) 159–164.